Chemistry of mycolactones, the causative toxins of Buruli ulcer

Yoshito Kishi[1]

Department of Chemistry and Chemical Biology, Harvard University, 12 Oxford Street, Cambridge, MA 02138

Edited by Stuart L. Schreiber, Broad Institute, Cambridge, MA, and approved January 13, 2011 (received for review November 3, 2010)

Buruli ulcer is a severe and devastating skin disease caused by *Mycobacterium ulcerans* infection, yet it is one of the most neglected diseases. The causative toxin, referred to as mycolactone A/B, was isolated and characterized as a polyketide-derived macrolide in 1999. The current status of the mycolactone chemistry is described, highlighting the stereochemistry assignment of mycolactone A/B; total synthesis; the structure determination of mycolactone congeners from the human pathogen *M. ulcerans*, the frog pathogen *Mycobacterium liflandii*, and the fish pathogen *Mycobacterium marinum*; the structural diversity in the mycolactone class of natural products; the highly sensitive detection/structure-analysis of mycolactones; and some biological activity.

structure elucidation | stucture diversity

Buruli ulcer, also known as Bairnsdale or Searle's ulcer, is a severe and devastating skin disease caused by *Mycobacterium ulcerans* infection, yet it is one of the most neglected diseases (Fig. 1). (1–4) Among the diseases caused by mycobacterial infection, Buruli ulcer occurs less frequently than tuberculosis (*Mycobacterium tuberculosis*) and leprosy (*Mycobacterium leprae*). However, it is noted that the occurrence of Buruli ulcer is increasing and spreading in tropical countries, and that the incidence of the disease may exceed that of leprosy and tuberculosis in highly affected areas. Infection with *M. ulcerans*, probably carried by aquatic insects (5) and mosquitoes (6), results in progressive necrotic lesions that, if untreated, can extend to 15% of a patient's skin surface. Surgical intervention has been the only practical curative therapy for Buruli ulcer. Encouragingly, combination treatments with rifampicin and either streptomycin or amikacin have recently been reported to prevent the growth of the bacteria in early lesions, pointing out the importance of diagnosing the disease at its preulcerative stage.

Most pathogenic bacteria produce toxins that play an important role(s) in disease. However, there has been no evidence thus far to suggest toxin production by *M. tuberculosis* and *M. leprae*. Interestingly, the presence of a toxin in *M. ulcerans* had been noticed for many years, but the toxin was not isolated until 1999 when Small and coworkers succeeded in isolation and characterization of two polyketide-derived macrolides from this bacteria (7). These macrolides were designated mycolactones A and B. However, under standard laboratory conditions, mycolactones A and B exist as a 3:2 equilibrating mixture and are referred to as mycolactone A/B in this paper.

Intradermal inoculation of mycolactone A/B into guinea pigs produces lesions similar to that of Buruli ulcer in humans, demonstrating their direct correlation with Buruli ulcer (8).

Structure

Gross Structure. The gross structure of mycolactone A/B was elucidated by Small and coworkers via a variety of spectroscopic methods; coupled with MS, UV, and IR studies, extensive 2D NMR experiments (GMQCOSY, TOCSY, HSQC, HMQC, and ROESY) led them to suggest the gross structure of mycolactone A/B (Fig. 2). Mycolactone A/B exists as a 3:2 equilibrating mixture, with the major and minor components corresponding to the

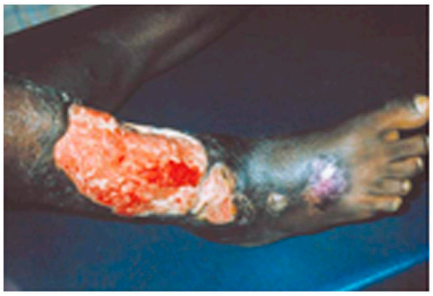

Fig. 1. Buruli ulcer lesion. Taken from "Buruli ulcer: *Mycobacterium ulcerans* infection", ed. Kingsley Asiedu, Robert Scherpbier, and Mario Raviglione, World Health Organization, 2000.

Z-$\Delta^{4',5'}$- and E-$\Delta^{4',5'}$-isomers, respectively, in the unsaturated fatty acid side chain (9).

Stereochemistry. There are 1,024 stereoisomers possible for the proposed gross structure of mycolactone A/B. Considering the limited availability, as well as the noncrystallinity of mycolactone A/B, we were aware of the difficulties which might be encountered in the assignment of its stereochemistry. Interestingly, we were then engaged in the development of the universal NMR database approach to assign the relative and absolute configuration of unknown compounds without degradation or derivatization (10). We recognized that the universal NMR database approach was uniquely suited to address the stereochemistry of the mycolactone A/B, and began the work.

In order to assign the relative stereochemistry at C16, C17, and C19, we wanted to learn the NMR profile for each diastereomer arising from these three stereogenic centers. For this purpose, we selected compound **1** corresponding to the C14-C20 moiety of mycolactone A/B (Fig. 3). All of the four possible diastereomers of **1** were synthesized, and their NMR properties were analyzed. This study demonstrated that: (*i*) each diastereomer exhibits a distinct NMR profile that differs from that of the other diastereomers and (*ii*) only diastereomer **1a** exhibits a profile matching the NMR profile of the C14-C20 portion of mycolactone A/B. Based on this observation, we predicted the relative stereochemistry at C16, C17, and C19 of mycolactone A/B corresponds to that of **1a**.

To address the relative stereochemistry at the macrolide moiety, i.e., C5, C6, C11, and C12, we adopted a similar, but slightly modified approach, considering the overall efficiency of work. These efforts led us to conclude the relative stereochemistry of the core to be **2** (Fig. 4).

Author contributions: Y.K. designed research; Y.K. performed research; Y.K. analyzed data; and Y.K. wrote the paper.

The authors declare no conflict of interest.

This article is a PNAS Direct Submission.

[1]To whom correspondence should be addressed. E-mail: kishi@chemistry.harvard.edu.

This article contains supporting information online at www.pnas.org/lookup/suppl/doi:10.1073/pnas.1015252108/-/DCSupplemental.

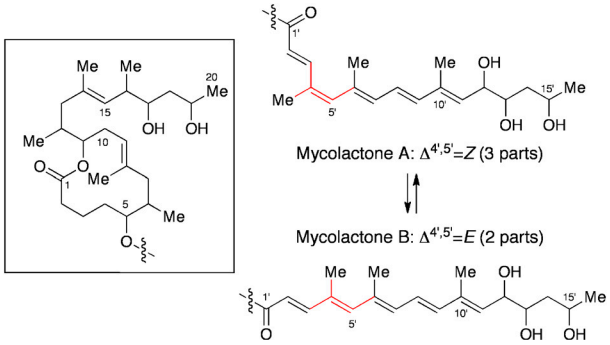

Fig. 2. Gross structure of mycolactone A/B. Mycolactone A/B exists as a 3:2 equilibrating mixture, with the major and minor components being *Z*-$\Delta^{4',5'}$- and *E*-$\Delta^{4',5'}$-isomers, respectively, in the unsaturated fatty acid side chain.

The absolute stereochemistry of the core was concluded from the comparison of the ^{1}H NMR spectra of the (*S*)- and (*R*)-Mosher esters prepared from **2** with those prepared from the core derived from natural mycolactone. We should note that, with the use of chiral NMR solvents developed later, the absolute configuration of the core could be determined only from NMR experiments (11).

To elucidate the NMR profile for each diastereomer arising from the three stereogenic centers at C12′, C13′, and C15′, we constructed an NMR database for compound **3**, e.g., synthesized all of the four possible diastereomers and analyzed their NMR properties. As anticipated, this experiment demonstrated that: (*i*) each diastereomer exhibits a distinct NMR profile that differs from that of the other diastereomers and (*ii*) the diastereomer **3** exhibits a profile matching the profile of this moiety of mycolactone A/B. From this observation, we predicted that the relative stereochemistry of mycolactone A/B at C12′, C13′, and C15′ corresponds to that of **3**.

With the relative stereochemistry determined, we attempted to establish the absolute configuration of the unsaturated fatty acid chain. Derivatization and degradation approaches proved unsuccessful, largely due to the very limited availability of the natural mycolactone. Under this circumstance, we recognized the potential of the NMR database approach in *chiral* solvents, which was concurrently developed in our laboratory (12). Thus, we studied the ^{1}H NMR profiles of the four diastereomers of **3** in (*R*)- and (*S*)-*N*, and α-dimethylbenzylamines [PhCH(Me)NHMe, DMBA], thereby revealing two important aspects. First, each diastereomer exhibited almost identical NMR profiles in both (*R*)- and (*S*)-DMBA, but very distinct and different NMR profiles from each other, thereby showing that the ^{1}H NMR database in (*R*)- and/or (*S*)-DMBA can be used for predicting the *relative* configuration of the structure motifs such as **3**. Second, each diastereomer exhibited a small but definitive difference between the chemical shifts recorded in (*R*)-DMBA and (*S*)-DMBA, demonstrating that the NMR database in (*R*)- and/or (*S*)-DMBA can be used for predicting the *absolute* configuration of the structure motifs such as **3**.

The ^{1}H NMR spectra of mycolactone A/B were recorded in (*R*)- and (*S*)-DMBA, and the chemical shift assignment was made through COSY experiments. The ^{1}H chemical shift differences ($\Delta\delta = \delta_R - \delta_S$) for the relevant protons in the natural mycolactone were found opposite in sign to those observed for **3**, allowing

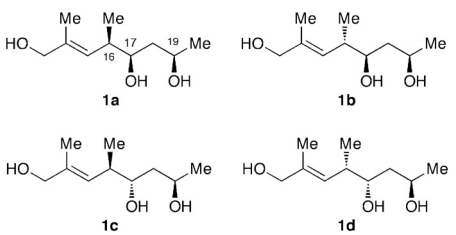

Fig. 3. Four diastereomers possible for the NMR database compound **1**.

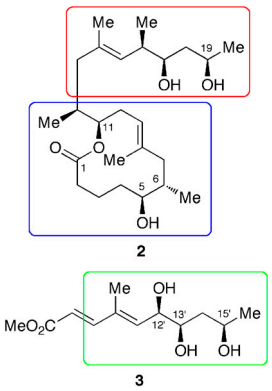

Fig. 4. Three structural motifs used for the stereochemistry assignment of mycolactone A/B. The structural motifs indicated in red and blue were used for the analysis of the core, whereas that in green was used for the analysis of the unsaturated fatty acid side chain.

us to establish that the C12′, C13′, and C15′-absolute configuration of the mycolactones corresponds to the antipode of **3**. Combined with the defined core structure, we concluded that the complete structure of the mycolactone A/B is **4** (Fig. 5) (13).

It is worthwhile adding that we were able to make the chemical shift assignment and determine the chemical shift differences ($\Delta\delta = \delta_R - \delta_S$) for the H17 and H19 protons. The experiment permitted us to predict that the absolute configuration of the core corresponds to that of **2**. This prediction was consistent with our earlier conclusion derived from the NMR analysis of the Mosher esters.

Structure Determinations of Mycolactone Congeners. Following the isolation of mycolactone A/B, several mycolactone congeners were reported from clinical isolates of *M. ulcerans* from Africa, Malaysia, Asia, Australia, and Mexico. In addition, mycolactone-like metabolites were isolated from the frog pathogen *Mycobacterium liflandii* and the fish pathogen *Mycobacterium marinum*. As these metabolites were available only in very minute quantities, their structure determination posed a major challenge. For many of these metabolites, the molecular formula estimated by mass spectroscopy was the only structure information available.

With a complete structure and a flexible, modular synthesis (*vide infra*) of mycolactone A/B, we took a new approach to establish the complete structure of the mycolactone congeners. To illustrate this approach, we shall use the case of mycolactone F isolated from the fish pathogen *M. marinum* (14).

Based on the mass spectroscopic data, Leadlay suggested the gross structure of mycolactone F (15). However, no data was available to assign its stereochemistry. Considering the similarity of mycolactone F to mycolactone A/B, we speculated **5** to be the likely structure and decided to synthesize this candidate (Fig. 6). Following the synthesis outlined later, we uneventfully obtained synthetic **5**. Under standard laboratory conditions, **5** (λ_{max} 323 nm, MeOH) did not isomerize as rapidly as mycolactone A/B (λ_{max} 362 nm, MeOH). Under photochemical condi-

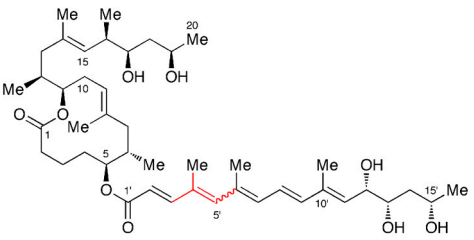

Fig. 5. Complete structure of mycolactone A/B. A wavy line indicates that this bond exists as a mixture of *E*- and *Z*-geometrical isomers.

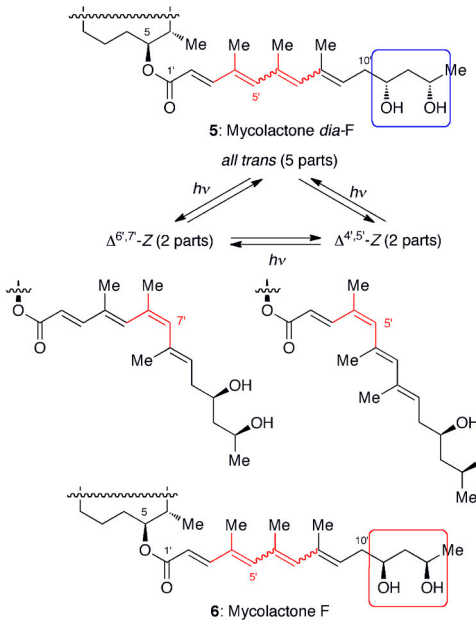

Fig. 6. Structure of mycolactones F and *dia*-F isolated from *M. marinum* DL240490 (cultured European sea bass) and BB170200 (freshwater silver perch), respectively. For the structure of core, see Fig. 5. Under the photochemical condition (300 nm, acetone), both mycolactones smoothly isomerize, to furnish a 5:2:2 mixture of three predominant regioisomers. A wavy line indicates that this bond exists as a mixture of *E*- and *Z*-geometrical isomers.

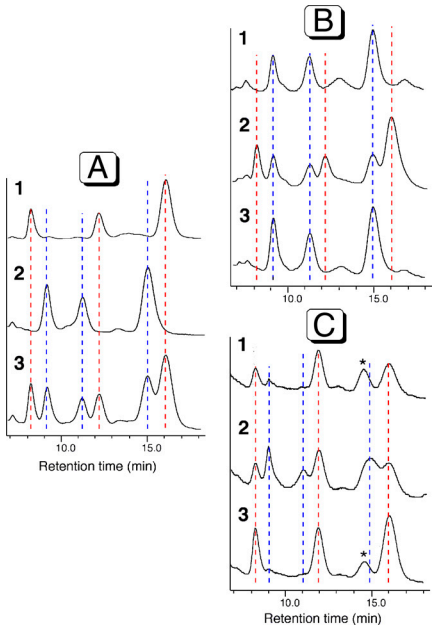

Fig. 7. HPLC comparison of synthetic, photochemically isomerized mycolactone F and *dia*-F with the mycolactones isolated from *M. marinum* in freshwater and saltwater fish. (*A*) 1: synthetic mycolactone F, 2: synthetic mycolactone *dia*-F, 3: their 1:1 mixture. (*B*) 1: mycolactone isolated from freshwater fish pathogen (*M. marinum* BB170200), 2: mixed with synthetic mycolactone F; 3: mixed with synthetic mycolactone *dia*-F. (*C*) 1: mycolactone isolated from saltwater fish pathogen (*M. marinum* DL240490), 2: mixed with synthetic mycolactone *dia*-F; 3: mixed with synthetic mycolactone F.

tions (300 nm, acetone), however, a facile geometric isomerization was observed, furnishing a 5:2:2 mixture of three predominant isomers-note the 1,3,5-trimethyl groups present in the chromophore of mycolactone F vs. the 1,3-dimethyl groups in the chromophore of mycolactone A/B. The ^{1}H NMR spectrum of synthetic, photochemically equilibrated material appeared to match the ^{1}H NMR spectrum reported for the natural mycolactone, which might suggest the structure of mycolactone F to be **5**. At the same time, we realized that this comparison alone could not exclude the possibility of **6**.

In our terminology, **6** is a remote diastereomer of **5**, a diastereomer due to the stereocenter(s) present outside a self-contained box(es) (16). As demonstrated in the universal NMR database work, remote diastereomers exhibit virtually identical, or at least very similar, NMR spectra in an achiral NMR solvent (17). However, in a chiral environment, they could show different physicochemical properties.

With both diastereomers **5** and **6** secured by synthesis, we began to search for an analytical method to distinguish them. Given the fact that only a very minute amount of natural mycolactone F was available, we needed an analytical method with a high sensitivity and opted to use chiral analytical HPLC. For this search, we purposely used the photochemically equilibrated **5** and **6** with the hope that each of their geometric isomers might give a distinct retention time. Thus, HPLC comparison could be performed on the basis of six, instead of two, distinct retention times-note that both **5** and **6** exist as a mixture of three predominant geometric isomers. After numerous attempts, we eventually found that a Chiralpak IA chiral column employing a mobile phase of toluene-isopropanol can distinguish all of the six remote diastereomers (Fig. 7). Finally, we subjected the natural product to this analysis, thereby demonstrating that mycolactone from the fish pathogen *M. marinum* is surprisingly **6** (18).

The 1,3-diol present in the unsaturated fatty acid side chain of **6** occurs curiously in the mirror image of the 1,3-diol present in other mycolactones. The mycolactone F used for this study was isolated from *M. marinum* DL240490 from cultured European sea bass. Intriguingly, we later found that the mycolactone isolated from *M. marinum* BB170200 from freshwater silver perch in Israel corresponds to **5**, referred to as mycolactone *dia*-F (19). In this light, it is interesting to quote the Stinear claim that mycolactone-producing mycobacteria have all evolved from a common *M. marinum* progenitor (20). This suggestion may imply that, at some stage of evolution, the absolute configuration in question was switched between the mycolactone F and mycolactone A/B series. Interestingly, prior to the isolation of mycolactone F from marine fish populations, all of the other mycolactones had been isolated from species located in or around freshwater habitats.

The approach described for the structure elucidation of mycolactone F was applied to establish the structure of mycolactones C (21, 22), D (23), E (24–26), and E ketone (27) (Fig. 8). Because this approach required an authentic sample for a given mycolactone, we needed to synthesize all of the mycolactones and their remote diastereomers. There was obviously an additional motivation for us to undertake the synthetic work, namely to learn the biological profiles of these mycolactones and their remote diastereomers.

Total Synthesis

As the structure of mycolactone A/B was elucidated by application of the newly developed logic and method, we felt it was important to confirm the assigned structure. For this reason, we carried out a total synthesis of mycolactone A/B and were able to confirm that the assigned structure was indeed correct (28). During the work, we realized that organic synthesis could play an additional, critical role to advance the mycolactone science. Because of the slow growth of *M. ulcerans*, it has been a difficult task to secure mycolactone A/B in quantities by fermentation. In addition, mycolactone A/B from the natural source is often contaminated with various unknown compounds, including mycolactone congeners. We believed that organic synthesis could supply homogeneous material in sufficient quantities for further study. With this analysis, we continued synthetic work and devel-

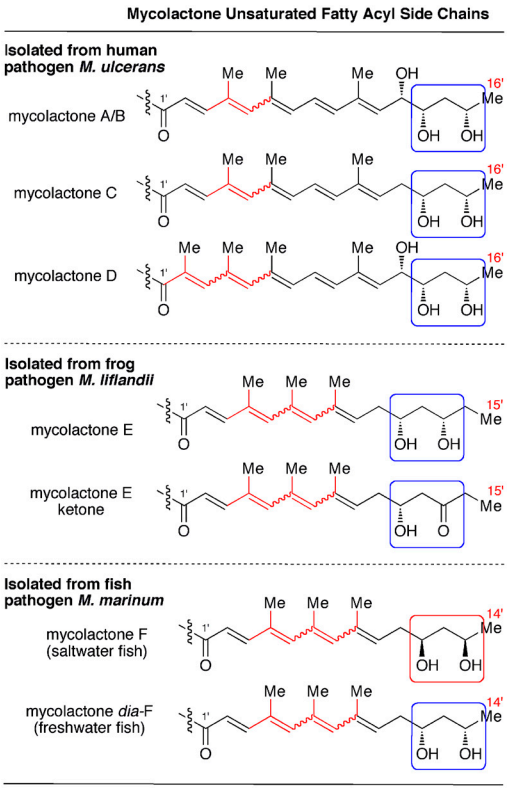

Fig. 8. Structurally well defined mycolactones. For the structure of core, see Fig. 5. A wavy line indicates that this bond exists as a mixture of *E*- and *Z*-geometrical isomers.

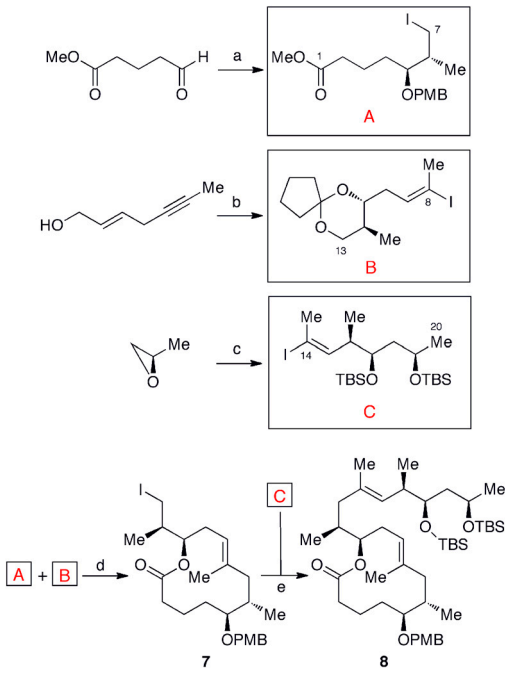

Fig. 9. Convergent synthesis of the core **8**. (*A*). The C5 and C6 stereogenic centers are incorporated by Brown crotylboration. (*B*). The C11 and C12 stereogenic centers are incorporated by Sharpless asymmetric epoxidation, followed by a regiospecific epoxide-opening with $LiCu(Me)_2$. (*C*). The C16 and C17 stereogenic centers are incorporated by Katsuki asymmetric epoxidation, followed by a regiospecific epoxide-opening with $Al(Me)_3$/MeLi. (*D*). Negishi cross coupling, followed by Yamaguchi lactonization. (*E*). Negishi cross coupling.

oped a scalable and efficient synthesis of the mycolactone class of natural products. In this section, we give a brief summary of the third generation synthesis (29). This synthesis is modular in nature and can be adjusted for the preparation of various mycolactone stereoisomers and/or analogs.

Core Synthesis. Fig. 9 summarizes the current core synthesis with the key synthetic reactions indicated. The core is assembled from the three building blocks **A**, **B**, and **C**, each of which is synthesized using asymmetric reactions such as Brown crotylboration, Sharpless asymmetric epoxidation, and Katsuki asymmetric epoxidation as the key steps. The building blocks **A**, **B**, and **C** are then assembled with Negishi cross-coupling reactions to furnish the mycolactone core **8**.

With this route, we have prepared 6 g of the mycolactone core with relative ease and anticipate that it should be straightforward to prepare even larger quantities, if the need arose. It is worthwhile noting: (*i*) this synthesis gives the core with >99% optical purity and (*ii*) this synthesis is flexible and permits access to various stereoisomers and analogs of the mycolactones.

Unsaturated Fatty Acid Synthesis. Fig. 10 summarizes the synthesis of the unsaturated fatty acid **9** from the building blocks **D** and **E** via Horner-Emmons reaction, followed by saponification (30). Under standard laboratory conditions, the pentaenoate obtained from the Horner-Emmons reaction rapidly equilibrates into a 3:2 mixture of the Z-$\Delta^{4',5'}$- and E-$\Delta^{4',5'}$-geometric isomers, which corresponds to the ratio of mycolactone A/B.

The phosphonate **D** was prepared from 2-butene-1,4-diol in stereochemically homogeneous form, whereas the aldehyde **E** was synthesized from commercially available, optically pure ethyl (*S*)-3-hydroxybutyrate. Sharpless asymmetric dihydroxylation was used to install the remaining hydroxyl groups of mycolactone A/B, whereas catalytic asymmetric Cr-mediated allylation was used to install the hydroxyl groups of mycolactones C, E, and F.

The coupling of the unsaturated fatty acid with the core was uneventfully accomplished using the Yamaguchi method, and subsequent tetrabutylammonium fluoride (TBAF)-promoted deprotection of the *tert*-butyldimethylsilyl (TBS) groups furnished mycolactone A/B. In the first generation synthesis, the C17/C19-diol of the core was protected as a cyclopentylidene ketal, but we noticed that the acid-promoted deprotection of the cyclopentylidene ketal was problematic. In contrast, mycolactone A/B is stable under the TBAF-promoted TBS-deprotection.

The mycolactones have attracted considerable attention from the synthetic community not only for their biological activity, but also for being the first examples of polyketide macrolides isolated from a human pathogen. Indeed, several other groups have reported the syntheses of mycolactone core and/or unsaturated fatty acid side chain (31–34).

Structural Diversity in the Mycolactone Class of Natural Products

All of the mycolactones reported to date are composed of a 12-membered macrolactone and a highly unsaturated fatty acid side chain. The macrolactone core is conserved in all of the members in the mycolactone class of natural products. On the other hand, there is a remarkable structural diversity observed in the unsaturated fatty acid portion, including the length of fatty acid backbone, the degree of unsaturation, the degree of hydroxylation, the stereochemistry of hydroxylation, the oxidation state of alcohols, and the number of methyl groups.

Three mycolactones A/B, C, and D from clinical isolates of *M. ulcerans* are structurally well defined. All of them are composed of a hexadecanoic acid backbone with a pentaenoate chromophore, but differ in the number of hydroxyl and methyl groups.

Two mycolactones from the frog pathogen *M. liflandii* are composed of a pentadecanoic acid backbone with the tetraenoate chromophore, but are different in the oxidation level, i.e., 1,3-diol vs. 1,3-hydroxyketone at C11′ and C13′. Mycolactones isolated

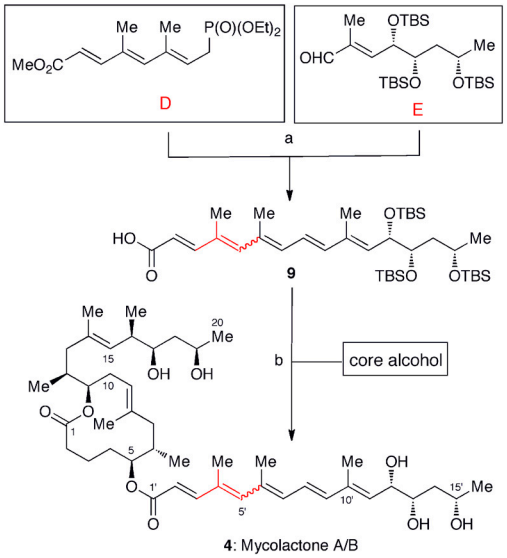

Fig. 10. Convergent synthesis of unsaturated fatty acid side chain and completion of total synthesis. Aldehyde **E** was synthesized from commercially available, optically pure ethyl (*S*)-3-hydroxybutyrate. Sharpless asymmetric dihydroxylation was employed for incorporation of the C11′ and C12′ stereogenic centers of mycolactones A/B and D, whereas asymmetric Cr-mediated allylation was employed for incorporation of the 1,3-diols of mycolactones C, E, F, and *dia*-F. (*A*). Horner-Emmons reaction, followed by saponification. (*B*). Yamaguchi esterification, followed by TBS deprotection with TBAF. A wavy line indicates that this bond exists as a mixture of *E*- and *Z*-geometrical isomers.

from pathogens of frogs are different from those of human pathogens in the length of the carbon backbone and the degree of unsaturation.

Mycolactones F and *dia*-F from the fish pathogen *M. marinum* share the same pentadecanoic acid. However, because the fatty acid occurs as a mirror image, mycolactones F and *dia*-F are remote diastereomers. All of the mycolactones known to date have the same absolute configuration of the 1,3-diol as that of mycolactone *dia*-F. The reason for the heterogeneity in the absolute configuration of the 1,3-diol moiety is not clear at this time, but it gives an additional dimension to the structural diversity of mycolactones. Mycolactones isolated from fish and human pathogens are different in the length of the carbon backbone and the degree of unsaturation.

Detection and Structure Analysis

As mentioned before, combination treatments with rifampicin and either streptomycin or amikacin have recently been reported to prevent the growth of the bacteria in early lesions, pointing out the importance of diagnosing the disease at its preulcerative stage. Currently, polymerase chain reaction of *M. ulcerans* DNA is commonly used to detect *M. ulcerans* infection (35). Undoubtedly, there is an urgent need for development of a cost and time effective method, ideally simple enough for field-use in remote areas, to detect *M. ulcerans* infection. Interestingly, mycolactone A/B appears to be biosynthetically restricted to *M. ulcerans* and homogeneously distributed within the infected tissue (36, 37). Based on this knowledge, we recognized the possibility of using mycolactones as a marker to detect *M. ulcerans* infection and/or diagnose Buruli ulcer.

Mycolactone A/B is known to behave well to thin-layer chromatography (TLC), thereby suggesting that TLC could potentially meet the need, except for the sensitivity of detection. With this analysis, we studied and developed a naphthylboronate-assisted fluorogenic chemosensor that can detect as low as 2 ng of mycolactone A/B in a semiquantitative manner (38). Relying on the excitation/emission of the pentaenoate chromophore, this method allows us to detect all of the mycolactones originating from the *human* pathogen *M. ulcerans*, but not mycolactones from the *fish* pathogen *M. marinum* or *frog* pathogen *M. liflandii*. For mycolactones derived from frogs and fish, the chiral HPLC profile should be a useful marker to detect their presence in fish tissue, for example.

We recognize two possible areas to apply the boronate-assisted fluorogenic chemosensor. First, this method appears to be suited for the mycolactone-based chemotaxonomy of *M. ulcerans*. To illustrate the feasibility of this method, we analyzed the crude lipid extracts of African and Australian strains of *M. ulcerans* (Fig. 11). Obviously, this method can be used: (*i*) to test the homogeneity of mycolactones and (*ii*) to detect new mycolactones.

Second, as mentioned in the introduction, we began this study with the hope of developing a cost and time effective method, ideally simple enough for field-use in remote areas, to detect *M. ulcerans* infection. To this end, we have shown that this method can detect mycolactone A/B in pig and fish skin and muscle tissues doped with mycolactone A/B. There are a few issues still to address, but we are cautiously optimistic in achieving the ultimate goal. We should note that this method is "invasive" in nature. To the best of our knowledge, however, an effective biological detection method, like tuberculin skin test for *M. tuberculosis* infection, is not yet developed to detect *M. ulcerans* infection. In addition, a long-lasting vaccine is not yet available to protect against Buruli ulcer.

Biological Activity

Various in vitro and in vivo studies in mice and guinea pigs demonstrated that mycolactone plays a central role in the pathogenesis of *M. ulcerans* disease; injection of 100 μg of the toxin was sufficient to cause characteristic ulcers in guinea pig skin (8). Mycolactone was shown to be associated with vacuolar nerve tissue damage in mice, which may account for the painlessness of Buruli ulcer lesions (39).

Significant progress has been made in the characterization of the biological activity of mycolactones, including cytotoxic and immunosuppresive effects (40). However, as it is beyond the scope of this article to make a comprehensive summary, we make only a few comments on the biological activity of mycolactones. Mycolactone A/B causes a cytopathic effect on mouse fibroblast L929 cells characterized by cytoskeletal rearrangement with rounding up and subsequent detachment from tissue culture plates. Mycolactone A/B causes cell cycle arrest at the G0/G1 phase, leading to cell death by apoptosis. It was noted that different cell lines vary in their sensitivity to the cytotoxicity of mycolactone A/B.(8) To the best of our knowledge, there is no cytotoxicity profile of mycolactones against a collection of human tumor cell lines. Yamori of The Cancer Chemotherapy Center of Japanese Foundation for Cancer Research conducted such an assay on synthetic mycolactone A/B (see Fig. S1), thereby showing a remarkable selectivity for LOX-IMVI cell-line.

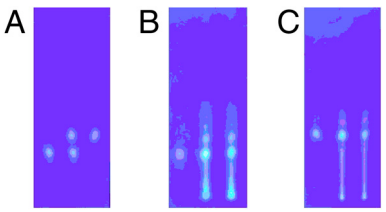

Fig. 11. TLC detection of mycolactones A/B and C. **Photograph A**: synthetic mycolactones A/B (left), C (right), and their mixture (center). **Photograph B**: synthetic mycolactone A/B (left), a lipid extract of an African strain of *M. Ulcerans* (right), and their mixture (center). **Photograph C**: synthetic mycolactone C (left), a lipid extract of an Australian strain of *M. Ulcerans* (right), and their mixture (center).

Thus far, structure-activity studies have been limited to only mycolactone A/B and its immediate derivatives (8, 41). Considering the structural diversity of natural mycolactones and the structural modifications now possible via organic synthesis, we can see an exciting opportunity to expand such structure-activity studies to shed further light on the molecular mechanisms of mycolactone action. A good departure point for this venture could be structure-activity studies on the natural mycolactones and their remote diastereomers (Fig. 8), that might uncover a relationship of a specific biological function with the minimum structural requirement. Once again, we should emphasize that these compounds are available as chemically well defined and homogeneous materials and also their structures can be tunable for the needs of investigations.

Despite efforts from many research groups, the molecular target of mycolactones remains unknown. In this connection, we should note that Jackson of our laboratory has recently synthesized analog **10a** (Fig. 12) and demonstrated that: (*i*) **10a** is useful to prepare a mycolactone conjugate and (*ii*) the amide **10b**, derived from **10a**, exhibits cytotoxicity (30 nm) against L929 fibroblasts in one third of the potency (10 nm) of mycolactone A/B.

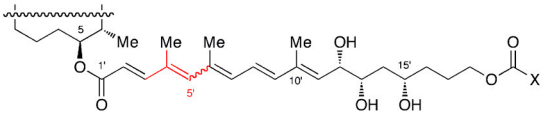

10a: X = $OC_6H_4NO_2$-*p*
10b: X = NHBu-*n*

Fig. 12. A possible precursor for preparation of mycolactone conjugates. For the structure of core, see Fig. 5. A wavy line indicates that this bond exists as a mixture of *E*- and *Z*-geometrical isomers.

Prospect

The chemistry of mycolactones, including structure determination/analysis, total synthesis, and highly sensitive detection methods, has been well developed. Because of the slow growth of *M. ulcerans*, it has been a major task to secure mycolactone A/B in quantities by fermentation. In addition, mycolactones from the natural sources are often contaminated with various unknown compounds, including their congeners. The scalable and flexible synthesis developed can now provide not only chemically well defined and homogeneous materials, but also mycolactone analogs for study. In our view, it is an exciting time to witness a new phase in the mycolactone science.

Cytotoxicity of synthetic mycolactone A/B against the 39 human tumor cell-lines is shown in the Fig. S1.

ACKNOWLEDGMENTS. We thank the National Institutes of Health (CA 22215) and Eisai USA Foundation for generous financial support.

1. Asiedu K, Scherpbier R, Raviglione M (2000) *Buruli ulcer: mycobacterium ulcerans infection*, eds K Asiedu, R Scherpbier, and M Raviglione (World Health Organization, Geneva).
2. Johnson PDR, et al. (2005) Buruli ulcer (*M. ulcerans* infection): new insights, new hope for disease control. *PLoS Med* 2:282–286.
3. Hong H, Demangel C, Pidot SJ, Leadlay PF, Stinear T (2008) Mycolactones: immunosuppressive and cytotoxic polyketides produced by aquatic mycobacteria. *Nat Prod Rep* 25:447–454.
4. Demangel C, Stinear TP, Cole ST (2009) Buruli ulcer: reductive evolution enhances pathogenicity of *Mycobacterium ulcerans*. *Nat Rev* 7:50–60.
5. Marsollier L, et al. (2002) Aquatic insects as a vector for *Mycobacterium ulcerans*. *Appl Environ Microb* 68:4623–4628.
6. Johnson PDR, et al. (2007) *Mycobacterium ulcerans* in mosquitoes captured during outbreak of Buruli ulcer, Southeastern Australia. *Emerg Infect Dis* 13:1653–1660.
7. George KM, et al. (1999) Mycolactone: a polyketide toxin from *Mycobacterium ulcerans* required for virulence. *Science* 283:854–857.
8. George KM, Pascopella L, Welty DM, Small PLC (2000) A *Mycobacterium ulcerans* toxin, mycolactone, causes apoptosis in guinea pig ulcers and tissue culture cells. *Infect Immun* 68:877–883.
9. Gunawardana G, et al. (1999) Characterization of novel macrolide toxins, mycolactones A and B, from a human pathogen, *Mycobacterium ulcerans*. *J Am Chem Soc* 121:6092–6093.
10. Kobayashi Y, Lee J, Tezuka K, Kishi Y (1999) Toward creation of a universal NMR database for the stereochemical assignment of acyclic compounds: the case of two contiguous propionate units. *Org Lett* 1:2177–2180.
11. Benewoitz AB, Fidanze S, Small PLC, Kishi Y (2001) Stereochemistry of the core structure of the mycolactones. *J Am Chem Soc* 123:5128–5129.
12. Kobayashi Y, Hayashi N, Tan C-H, Kishi Y (2001) Toward the creation of NMR databases in chiral solvents for assignments of relative and absolute stereochemistry: proof of concept. *Org Lett* 3:2245–2248.
13. Fidanze S, Song F, Szlosek-Pinaud M, Small PLC, Kishi Y (2001) Complete structure of the mycolactones. *J Am Chem Soc* 123:10117–10118.
14. Ranger BS, et al. (2006) Globally distributed mycobacterial fish pathogens produce a novel plasmid-encoded toxic macrolide, mycolactone F. *Infect Immun* 74:6037–6045.
15. Hong H, Stinear T, Porter J, Demangel C, Leadlay P (2007) A novel mycolactone toxin obtained by biosynthetic engineering. *ChemBioChem* 8:2043–2047.
16. Kobayashi Y, Tan C-H, Kishi Y (2000) Toward creation of a universal database for stereochemical assignment: the case of 1,3,5-trisubstituted acyclic systems. *Helv Chim Acta* 83:2562–2571.
17. Boyle CD, Harmange J-C, Kishi Y (1994) Novel structure elucidation of AAL Toxin T_A backbone. *J Am Chem Soc* 116:4995–4996.
18. Kim H-J, Kishi Y (2008) Total synthesis and stereochemistry of mycolactone F. *J Am Chem Soc* 130:1842–1844.
19. Kim H-J, et al. (2009) Heterogeneity in the stereochemistry of mycolactones isolated from *M. marinum*: toxins produced by fresh *vs.* saltwater fish pathogens. *Chem Commun* 7402–7404.
20. Yip MJ, et al. (2007) Evolution of *Mycobacterium ulcerans* and other mycolactone-producing mycobacteria from a common *Mycobacterium marinum* progenitor. *J Bacteriol* 189:2021–2029.
21. Mve-Obiang A, Lee RE, Portaels F, Small PLC (2003) Heterogeneity of mycolactones produced by clinical isolates of *Mycobacterium ulcerans*: implications for virulence. *Infect Immun* 71:774–783.
22. Judd TC, Bischoff A, Kishi Y, Adusumilli S, Small PLC (2004) Structure determinationof mycolactone C via total synthesis. *Org Lett* 6:4901–4904.
23. Hon H, Spencer JB, Porter JL, Leadlay PF, Stinear T (2005) A novel mycolactone from a clinical isolate of *Mycobacterium ulcerans* provides evidence for additional toxin heterogeneity as a result of specific changes in the modular polyketide synthase. *ChemBioChem* 6:643–648.
24. Mve-Obiang A, et al. (2005) A newly discovered mycobacterial pathogen isolated from laboratory colonies of *Xenopus* species with lethal infections produces a novel form of mycolactone, the *Mycobacterium ulcerans* macrolide toxin. *Infect Immun* 73:3307–3312.
25. Hong H, Stinear T, Skelton P, Spencer JB, Leadlay PF (2005) Structure elucidation of a novel family of mycolactone toxins from the frog pathogen *Mycobacterium sp* MU128FXT by mass spectrometry. *Chem Commun* 4306–4308.
26. Aubry S, et al. (2008) Synthesis and structure of mycolactone E isolated from frog mycobacterium. *Org Lett* 10:5385–5388.
27. Spangenberg T, Aubry S, Kishi Y (2010) Synthesis and structure assignment of the minor metabolite arising from the frog pathogen *Mycobacterium liflandii*. *Tetrahedron Lett* 51:1782–1785.
28. Song F, Fidanze S, Benowitz AB, Kishi Y (2002) Total synthesis of the mycolactones. *Org Lett* 4:647–650.
29. Jackson KL, Li W, Chen C-L, Kishi Y (2010) Scalable and efficient synthesis of the mycolactone core. *Tetrahedron* 66:2263–2272.
30. Song F, Fidanze S, Benowitz AB, Kishi Y (2007) Total synthesis of mycolactones A and B. *Tetrahedron* 63:5739–5753.
31. Alexander MD, et al. (2006) Synthesis of the mycolactone core by ring-closing metathesis. *Chem Commun* 4602–4604.
32. Feyen F, Jantsch A, Altmann K-H (2007) Synthetic studies on mycolactones: synthesis of the mycolactone core structure through ring-closing olefin metathesis. *Synlett* 415–418.
33. van Summeren RP, Feringa BL, Minnaard AJ (2005) New approaches towards the synthesis of the side-chain of mycolactones A and B. *Org Biomol Chem* 3:2524–2533.
34. Yin N, Wang G, Qian M, Negishi E (2006) Stereoselective Synthesis of the side chains of mycolactones A and B featuring stepwise double substitutions of 1,1-Dibromo-1-alkenes. *Angewandte Chemie International Edition* 45:2916–2920.
35. Eddyani M, et al. (2009) Fine-needle aspiration, an efficient sampling technique for bacteriological diagnosis of nonulcerative Buruli ulcer. *J Clin Microbiol* 47:1700–1704.
36. Hong H, et al. (2008) Mycloactone diffuses from *Mycobacterium ulcerans*-infected tissues and targets mononuclear cells in peripheral blood and lymphoid organs. *PLoS Neglect Trop D* e325:1–8.
37. Sarfo FS, et al. (2010) Detection of mycolactone A/B in *Mycobacterium ulcerans*-infected human tissue. *PLoS Neglect Trop D* 4:1–9.
38. Spangenberg T, Kishi Y (2010) Highly sensitive, operationally simple, cost/time effective detection of the mycolactones from the human pathogen *Mycobacterium ulcerans*. *Chem Commun* 46:1410–1412.
39. En J, et al. (2008) Mycolactone is responsible for the painlessness of *Mycobacterium ulcerans* infection (buruli Ulcer) in a murine study. *Infect Immun* 76:2002–2007.
40. Pahlevan AA, et al. (1999) The inhibitory action of *Mycobacterium ulcerans* soluble factor on monocyte/T cell cytokine production and NF-κB function. *J Immunol* 163:3928–3935.
41. Snyder DS, Small PLC (2003) Uptake and cellular actions of mycolactone, a virulence determinant for *Mycobacterium ulcerans*. *Microb Pathogenesis* 34:91–101.